The Roles of Radiative Forcing, Sea Surface Temperatures, and Atmospheric and Land Initial Conditions in U.S. Summer Warming Episodes

LIWEI JIA,*,+ GABRIEL A. VECCHI,+ XIAOSONG YANG,#,+ RICHARD G. GUDGEL,+ THOMAS L. DELWORTH,+ WILLIAM F. STERN,+ KAREN PAFFENDORF,+ SETH D. UNDERWOOD,@ AND FANRONG ZENG+

* *Princeton University, Princeton, New Jersey*
+ *NOAA/Geophysical Fluid Dynamics Laboratory, Princeton, New Jersey*
# *University Corporation for Atmospheric Research, Boulder, Colorado*
@ *Engility Corporation, Chantilly, Virginia*

(Manuscript received 9 July 2015, in final form 20 February 2016)

ABSTRACT

This study investigates the roles of radiative forcing, sea surface temperatures (SSTs), and atmospheric and land initial conditions in the summer warming episodes of the United States. The summer warming episodes are defined as the significantly above-normal (1983–2012) June–August 2-m temperature anomalies and are referred to as heat waves in this study. Two contrasting cases, the summers of 2006 and 2012, are explored in detail to illustrate the distinct roles of SSTs, direct radiative forcing, and atmospheric and land initial conditions in driving U.S. summer heat waves. For 2012, simulations with the GFDL atmospheric general circulation model reveal that SSTs play a critical role. Further sensitivity experiments reveal the contributions of uniform global SST warming, SSTs in individual ocean basins, and direct radiative forcing to the geographic distribution and magnitudes of warm temperature anomalies. In contrast, for 2006, the atmospheric and land initial conditions are the key drivers. The atmospheric (land) initial conditions play a major (minor) role in the central and northwestern (eastern) United States. Because of changes in radiative forcing, the probability of areal-averaged summer temperature anomalies over the United States exceeding the observed 2012 anomaly increases with time over the early twenty-first century. La Niña (El Niño) events tend to increase (reduce) the occurrence rate of heat waves. The temperatures over the central United States are mostly influenced by El Niño/La Niña, with the central tropical Pacific playing a more important role than the eastern tropical Pacific. Thus, atmospheric and land initial conditions, SSTs, and radiative forcing are all important drivers of and sources of predictability for U.S. summer heat waves.

1. Introduction

Excessive summer season warming has adverse social, environmental, and economic effects. For example, the 2003 European summer heat wave caused the death of over 70 000 people (Robine et al. 2008), forest fires (Fischer et al. 2007), and decreased agriculture production. It has been estimated that more than 800 deaths can be attributed to the 1995 mid-July heat wave over the central United States (Changnon et al. 1996). These multiday heat waves often sit within higher-than-normal seasonal mean temperature anomalies. It should be recognized that there exist no universal definitions for heat wave as it is relative to a specific area and to a certain time period (Robinson 2001; Perkins and Alexander 2013). According to the World Meteorological Organization (WMO), a heat wave ''event'' is defined as five or more consecutive days in which the average daily maximum temperature is exceeded by at least 5°C relative to the normal period of 1961–90 (Frich et al. 2002). Another commonly used definition for ''seasonal'' heat waves is based on seasonal or monthly mean temperature anomalies (Wang et al. 2014; Schubert et al. 2014; Stott et al. 2004; Schär et al. 2004; Dole et al. 2011). In the present study, we adopt the definition based on seasonal means, and a ''summer'' heat wave refers to the significantly above-normal (relative to 1983–2012) June–July–August (JJA) mean 2-m temperature anomalies.

Exploring the mechanisms of heat waves can help assess sources of predictability, and enable improved

Corresponding author address: Liwei Jia, NOAA/Geophysical Fluid Dynamics Laboratory, 201 Forrestal Rd., Princeton, NJ 08540.
E-mail: Liwei.Jia@noaa.gov

DOI: 10.1175/JCLI-D-15-0471.1

prediction and early response to a developing heat wave. Various mechanisms responsible for U.S. heat waves have been proposed in early studies (Wang et al. 2014; Hoerling et al. 2013; Koster et al. 2009; Dole et al. 2014; Hansen et al. 2012). The study by Dole et al. (2014) suggested that the extreme warmth over the central and eastern United States in March 2012 resulted primarily from natural internal climate and weather variability. Wang et al. (2014) highlighted the role of sea surface temperature (SST) forcing in the 2011 and 2012 U.S. summer heat waves. Hansen et al. (2012) concluded that heat waves, such as those in Texas and Oklahoma in the summer of 2011 were a consequence of human-made greenhouse gases. The role played by land–atmosphere interactions in U.S. heat waves has also been documented (Huang and Van den Dool 1993).

In spite of the studies on the physical mechanisms of U.S. heat waves, there are still substantial disagreements and unknowns on the role of large-scale processes, such as SST forcing and radiative forcing, in heat waves (Schubert et al. 2014). In this study, we attempt to draw together the possible mechanisms contributing to U.S. heat waves in summertime (JJA). The specific question considered here is the roles of atmospheric internal dynamics, land–atmosphere interactions, ocean boundary conditions (i.e., SSTs) and radiative forcing in U.S. summer heat waves. A suite of experiments with Geophysical Fluid Dynamics Laboratory (GFDL) Atmospheric General Circulation Model (AM2.5) and Forecast-oriented Low Ocean Resolution (FLOR) coupled climate models are designed to address the above question, with a focus on the spatial pattern and magnitudes of warm temperature anomalies over the United States due to SSTs in individual ocean basins, uniform global SST warming, direct radiative forcing, atmospheric and land initial conditions, as well as the probability of record threshold exceedance due to changes in radiative forcing.

The rest of the paper is organized as follows. Section 2 describes the model, experimental design, and data. The results are presented in section 3. The summary and discussion are provided in section 4.

2. Model, experimental design, and data

a. Model

The high-resolution coupled GFDL FLOR model was utilized in this study. The atmosphere and land components of FLOR are taken from GFDL high-resolution atmosphere–ocean Coupled Model version 2.5 (CM2.5; Delworth et al. 2012) with a horizontal resolution of ~0.5°, and 32 vertical levels. The ocean and sea ice components of FLOR are based on the low-resolution GFDL Coupled Model version 2.1 (CM2.1; Delworth et al. 2006; Wittenberg et al. 2006; Gnanadesikan et al. 2006) with a spatial resolution of ~1° and 50 vertical levels. A detailed description of this climate model was documented in Vecchi et al. (2014). It is one of the North American Multimodel Ensemble (NMME) models that provide real-time seasonal-to-interannual predictions (Kirtman et al. 2014; http://www.cpc.ncep.noaa.gov/products/NMME). FLOR has shown skillful predictions in tropical cyclones, extratropical storms, 2-m temperature, and precipitation over land (Vecchi et al. 2014; Murakami et al. 2015; Yang et al. 2015; Jia et al. 2015). We used the flux-adjusted version of the model, in which climatological adjustments were made to the model's momentum, enthalpy, and freshwater fluxes from atmosphere to ocean to bring the model's long-term climatology of SST and surface wind stress closer to observational estimates over 1979–2012 (Vecchi et al. 2014).

b. Experimental design

1) FLOR RETROSPECTIVE SEASONAL FORECASTS

A set of retrospective seasonal forecasts were conducted for FLOR (called phase-1 forecasts, hereafter referred to as p1) from 1981 to the present. The initial conditions of the ocean and ice components for FLOR forecasts were taken from the GFDL's ensemble coupled data assimilation (ECDA) system developed specifically for CM2.1 (Zhang et al. 2007; Zhang and Rosati 2010; Chang et al. 2013). The initial conditions for the atmosphere and land components were taken from the atmospheric model (AM2.5) simulations forced by observed SST and sea ice concentration. The observed SST and sea ice concentration dataset used to force AM2.5 was a merged product based on the monthly mean Hadley Centre Sea Ice and Sea Surface Temperature dataset version 1 (HadISST1) and version 2 of the National Oceanic and Atmospheric Administration (NOAA) weekly optimum interpolation (OI) SST analysis (Hurrell et al. 2008). Before 2005, FLOR was forced with observationally based estimate of changing concentrations of greenhouse gases, aerosols, land-use changes, solar irradiance variations, and volcanic aerosols. After 2005, FLOR was forced with estimates of changing greenhouse gases and aerosols based on the representative concentration pathway (RCP) 4.5 scenario (Meinshausen et al. 2011). For each forecast, 12 ensemble members were initialized on the first day of each month, and were integrated for 12 months. Each ensemble member was initialized with the ocean and sea ice initial conditions from each member of CM2.1 ECDA, and the atmospheric and land initial conditions were from three AM2.5 simulations generated offline.

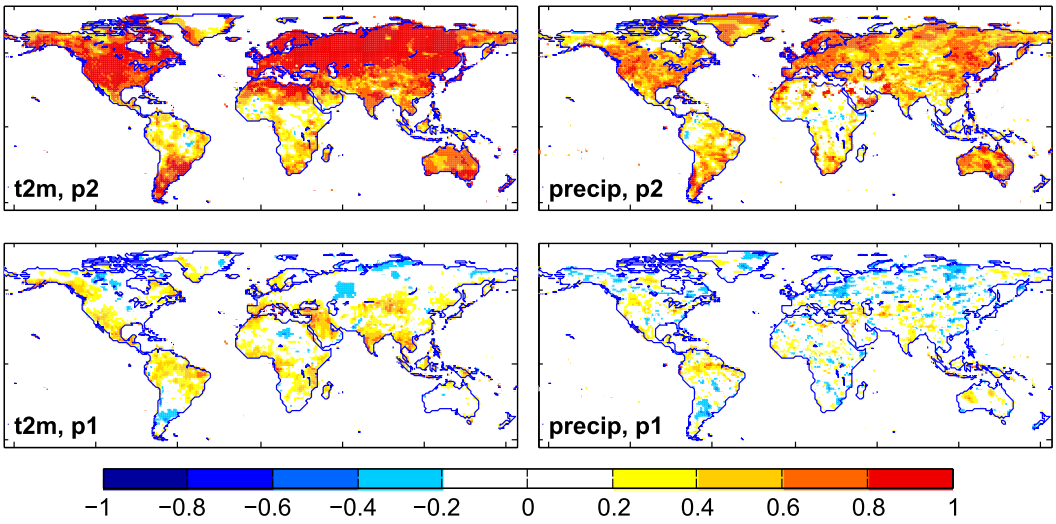

FIG. 1. The pointwise correlation coefficients of initial conditions of (left) 2-m temperature and (right) precipitation in June for FLOR phase-1 and -2 forecasts. The initial conditions are from 11-member mean of AM2.5 simulations for FLOR phase-1 forecasts, and from nudging process for FLOR phase-2 forecasts. The verification data used to calculate correlation coefficients are the GHCN gridded v2 2-m temperature over land at 0.5° resolution during 1983–2012 (Fan and Van den Dool 2008), and NOAA's precipitation reconstruction over land at 0.5° resolution (Chen et al. 2002) during 1983–2011.

The first AM2.5 member was applied to the first four ocean members, the second AM2.5 member was applied to ocean members from 5 to 8, and the third AM2.5 member was applied to ocean members from 9 to 12 (Vecchi et al. 2014).

Another set of ensemble retrospective forecasts (called phase-2 forecasts, hereafter referred to as p2) were conducted with identical configurations as p1, except that the surface pressure and the three-dimensional winds and temperature were nudged toward the Modern-Era Retrospective Analysis for Research and Applications (MERRA) 50-km resolution reanalysis (Rienecker et al. 2011) on a 6-hourly time scale. The nudging process started from 1979 to the present, and the outputs were used as atmospheric and land initial conditions for p2 forecasts. To avoid spinup issues, we analyzed p2 forecasts from 1983 to 2012. The atmospheric and land initial conditions are identical (from nudging process) for all 12 ensemble members, but the ocean and sea ice initial conditions are different (from ECDA) for each member. Because of the nudging procedure, the atmosphere and land initial conditions for p2 ought to be more realistic than those for p1, and the consequent predictive skill in p2 is expected to be improved over p1 as will be demonstrated later in this subsection. Both p1 and p2 ensemble retrospective forecasts during the period of 1983–2012 were analyzed in this study.

It is worth emphasizing that the predictive skill in p2 comes from ocean initialization, radiative forcing, plus atmospheric and land initial conditions. However, the predictive skill in p1 comes only from ocean initialization and radiative forcing, and no MERRA reanalysis (considered as ''observed'') information is integrated into the atmospheric and land initial conditions. The distinct difference between p1 and p2 forecasts is the observed atmospheric and land initial information.

To demonstrate the difference between p1 and p2 forecasts, we show in Fig. 1 the pointwise correlation coefficients of June initial conditions of 2-m temperature and precipitation for FLOR p1 and p2 forecasts. The initial conditions are from 11-member mean of AM2.5 simulations for p1, and from the nudging process for p2. The verification data used to calculate correlation coefficients are the Global Historical Climatology Network (GHCN) gridded v2 2-m temperature over land at 0.5° resolution during 1983–2012 (Fan and Van den Dool 2008), and NOAA's precipitation reconstruction over land at 0.5° resolution (Chen et al. 2002) during 1983–2011. The initial conditions of temperature and precipitation for p2 agree more with the observations than those for p1, as indicated by the considerably higher correlation coefficients in p2 over p1. This improved initial state is evident for the p2 forecasts, in fact, in all initial months (not shown). Furthermore, the overall predictive skill of 12-member mean JJA temperature and precipitation (initialized on 1 June) is higher in p2 than the skill in p1 (Fig. 2). The correlation coefficients in p2 are higher than those of p1 in most areas, such as the northern Asia, the eastern United States for temperature, and

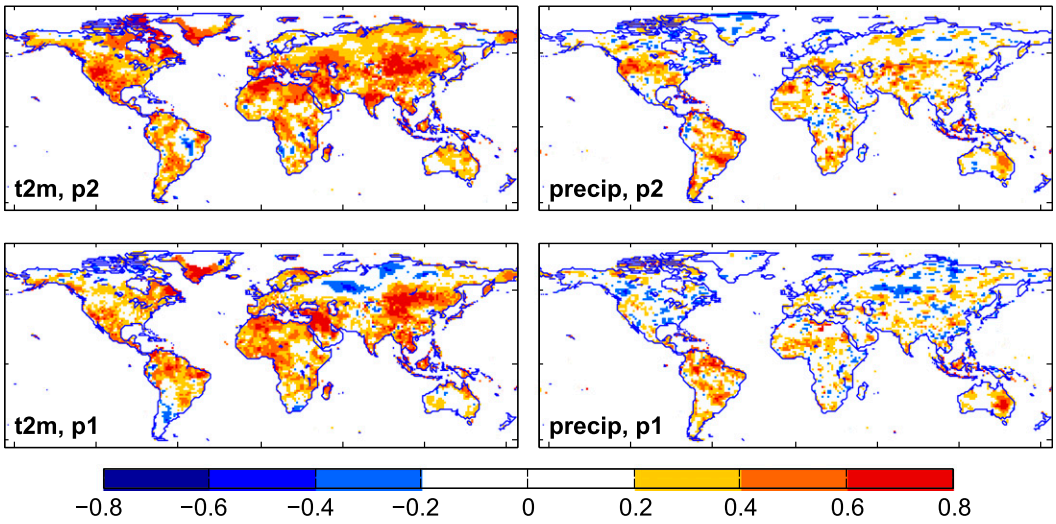

FIG. 2. The pointwise correlation coefficients of JJA (left) 2-m temperature and (right) precipitation from FLOR phase-1 and -2 retrospective forecasts initialized on 1 June. The observations of temperature and precipitation used here are identical to those used in Fig. 1.

North America for precipitation. Note that the correlation difference between p1 and p2 in June's initial state (Fig. 1) is greater than the difference in JJA forecasts, primarily because the latter is the difference of three-month (JJA) mean, rather than one-month mean (June). Little to no difference in correlation skill between p1 and p2 was found for July and August forecasts initialized on 1 June (not shown).

2) FLOR 30-ENSEMBLE HISTORICAL AND PROJECTION SIMULATIONS

A total of 30 members of FLOR simulations from 1941 to 2050 were used to identify long-term U.S. summer heat wave variations due to changes in radiative forcing. The anthropogenic and natural forcing before 2005 was prescribed based on observed historical record. From 2006 to 2050, the forcing was based on the RCP4.5 scenario.

3) AM2.5 BASELINE EXPERIMENT AND SENSITIVITY EXPERIMENTS

The 11-member AM2.5 simulations, forced with observed monthly mean SST and sea ice concentration (HadISST1/OI SST) and time-varying radiative forcing, were conducted for the period from 1979 to the present. These simulations are called AM2.5 baseline simulations to be distinguished from the sensitivity experiments described below.

We set up a series of sensitivity experiments with AM2.5 to examine the roles played by uniform global SST warming, direct radiative forcing, and SSTs in individual ocean basins in the 2012 U.S. summer heat wave. The first sensitivity experiment tests the impact of uniform global SST warming on the heat wave given that climate models project, to first order, a spatially uniform sea surface warming pattern. In the experiment, the global mean SST anomalies were removed from the observed monthly mean SSTs used to force AM2.5 (called the no-SST-warming experiment). Thus, the difference between this no-SST-warming experiment and the AM2.5 baseline simulations reveals the role of uniform global SST warming. The second sensitivity experiment is the same as the AM2.5 baseline simulations, but for the radiative forcing, agents were set to climatological values during 1983–2012, called climatological radiative forcing experiment (hereafter ClimRF). The difference between ClimRF and AM2.5 baseline simulations isolates the role of direct radiative forcing. Another four sensitivity experiments examine the influence of individual ocean basins in the 2012 U.S. summer heat wave, in which the AM2.5 is forced with monthly mean climatological SSTs everywhere but in selected ocean basins in question. We selected domains in the tropical Pacific (20°S–20°N), the North Pacific (20°–90°N), the North Atlantic (20°–90°N), and the tropical Atlantic (20°S–20°N). We omitted the Indian Ocean, because earlier studies have reported little impact of Indian Ocean SSTs on U.S. heat waves (Wang et al. 2014). In each of the four experiments, we removed global-averaged SST anomalies from the observed SST forcing data before perturbing the ocean basins in order to eliminate the role of uniform global SST warming in the heat wave. However, the radiative forcing in the four experiments was based on the time-varying historical

TABLE 1. List of experiments using AM2.5.

Name	Radiative forcing	SST forcing	Atmospheric/land initial conditions	Time period used	Ensemble size
1) Baseline	Time varying	Observed global	Started Jan 1979 with random Jan states	1983–2012	11
2) No-SST-warming	Time varying	Observed global (global mean warming anomalies removed)	Jan 2012 of baseline	Jan–Dec 2012	11
3) Climatological radiative forcing	Climatology (1983–2012)	As in 1)	Jan 2012 of baseline	Jan–Dec 2012	11
4) Ocean basin	Time varying	Tropical Atlantic (20°S–20°N) Tropical Pacific (20°S–20°N) North Atlantic (20°–90°N) North Pacific (20°–90°N) (Global mean warming anomalies removed)	Jan 2012 of baseline	Jan–Dec 2012	11 each
5) Ocean basin to generate climatologies	Time varying	As in 4)	Started Jan 1981 with Jan 1981 baseline states	1983–2012	2 each
6) No-SST-warming to generate climatologies	Time varying	As in 2)	As in 5)	1983–2012	2 each

data (i.e., the influence of direct radiative forcing was included), because the direct radiative forcing plays little role in the 2012 U.S. summer heat wave as will be demonstrated in the next section. A 10° buffer zone was included at the borders of each selected basin for a smoother transition. For instance, the 10°–20°N over the North Pacific was considered as the buffer zone for the North Pacific (20°–90°N) basin. Each sensitivity experiment consists of 11 ensemble members initialized on 1 January 2012, and integrated for 12 months. We analyzed the JJA mean 2-m temperatures from these experiments. To construct long-term climatology for sensitivity experiments, we also ran 30 years (1983–2012) for each sensitivity experiment but for the ClimRF, with two members for each year. Then, the climatology was estimated as the grand mean of the two members during 1983–2012. The climatology for ClimRF was estimated as the climatology of the AM2.5 baseline simulations. The complete set of experiments using AM2.5 is listed in Table 1.

4) FLOR PHASE-2 SENSITIVITY EXPERIMENTS

Two sets of sensitivity experiments exploring the individual roles of atmospheric and land initial conditions in the 2006 U.S. summer heat wave were designed utilizing the FLOR p2 forecast system. In the experiment, the atmospheric (land) initial conditions of June 2006 in FLOR p2 were taken from June initial states of random years to minimize the contributions of atmospheric (land) initial information to seasonal forecasts, hereafter called no-atmos-ICs (no-land-ICs). We chose initial conditions from three random years and generated 36 ensemble members, with 12 members from each random year. The results we show in this study are based on the 36-member mean. The difference between the original p2 baseline forecasts and the forecasts from the no-atmos-ICs (no-land-ICs) experiment represents the role of atmospheric (land) initial conditions. The two sensitivity experiments were initialized on 1 June 2006 and integrated for 12 months. Initializing in June is expected to yield higher predictive skill than initializing earlier than June for the predictions of JJA, which is the season we focus on. Since there was only one year (June 2006–May 2007) forecasts from each sensitivity experiment, the anomalies of the sensitivity experiments were computed by subtracting the 30-yr climatology (1983–2012) of the p2 baseline forecasts. A list of the experiments using FLOR p2 is shown in Table 2. In baseline and sensitivity experiments, time-varying radiative forcing was used, and the ocean and sea ice initial conditions were from ECDA. Because the role of atmospheric/land initial conditions was estimated by taking the difference between the p2 baseline forecasts and the forecasts from sensitivity experiment (both have time-varying radiative forcing), the effects of radiative forcing were cancelled out.

c. Data

The GHCN gridded v2 2-m temperature over land at 0.5° resolution (Fan and Van den Dool 2008) is used for verification purpose. We also use the precipitation at 0.5° from NOAA's precipitation reconstruction over land (Chen et al. 2002), the version-2 Global Precipitation Climatology Project (GPCP) monthly precipitation dataset at 2.5° resolution (Adler et al. 2003, provided by the NOAA/OAR/ESRL PSD, Boulder, Colorado;

TABLE 2. List of experiments using FLOR phase 2.

Name	Atmospheric initial conditions	Land initial conditions	Time period used	Ensemble size
1) Baseline	First day of each month	First day of each month	1983–2012	12
2) No-land-ICs	1 Jun 2006	Random 1 Jun	Jun 2006–May 2007	36
3) No-atmos-ICs	random 1 Jun	1 Jun 2006	As in 2)	36

http://www.esrl.noaa.gov/psd/), 500-hPa height from MERRA reanalysis (Rienecker et al. 2011), and soil moisture content from the Global Land Data Assimilation Systems (GLDAS) Noah V3.3 (Rodell et al. 2004). The observed SST data are from HadISST1 (Rayner et al. 2003).

3. Results

The summers (JJA) of 2006, 2011, and 2012 over the U.S. were three warmest summers during 1983–2012, with observed areal-averaged 2-m temperature anomalies above 0.8° (Fig. 3). In this study, the U.S. domain was simply defined as the continental areas within 30°–50°N and 130°–60°W. We will show shortly that SSTs are important for the warm summers of 2011 and 2012, while atmospheric and land initial conditions are principal factors for the summer of 2006. We chose the summers of 2012 and 2006 as two contrasting cases to illustrate the roles played by SSTs, atmospheric, and land initial conditions. In the last part of this section, we also examine the contributions of changes in radiative forcing to multidecadal variations of U.S. summer heat waves from 30-member FLOR simulations during 1941–2050.

Figure 4 shows the 2012 JJA 2-m temperature anomalies (relative to 1983–2012) over the continental United States from the observations, ensemble mean of AM2.5 baseline simulations, and FLOR p1 and p2 forecasts initialized on 1 June 2012. The observed positive temperature anomalies over the United States are well captured in the AM2.5 baseline simulations, FLOR p1, and FLOR p2 forecasts with a pattern correlation of 0.51, 0.48, and 0.60, respectively. Because the AM2.5 baseline simulations are forced by observed SSTs, the fact that AM2.5, forced by SSTs alone, captures the observed heat wave implies that SSTs are critical for the 2012 U.S. summer heat wave. Similarly for the summer of 2011, SSTs play a dominant role in the warm temperature anomalies of the United States (not shown). Moreover, the spatial structure of temperature anomalies from p2 forecasts shows more similarities to the observations than p1, as suggested by the higher pattern correlation in p2 (0.60) over p1 (0.48). The improved forecasts in p2 over p1 reveal that atmospheric and land initial information also plays a certain role in the 2012 U.S. summer heat wave, because the difference between p2 and p1 forecasts is the improved atmospheric and land initial conditions in p2 over p1 (see Fig. 1). We note that the temperature anomalies over the northeastern United States are overestimated in p2, which might be related to the overestimation of JJA temperature variability over northeastern United States in p2 (not shown). However, diagnosing the source of such temperature bias is beyond the scope of this study. It is worth mentioning that the time-varying radiative forcing agents were used in the AM2.5 baseline simulations and FLOR p1 and p2 forecasts. The role of radiative forcing in temperature anomalies is included in the above results. However, we will show below that the direct radiative forcing plays little role in the 2012 U.S. JJA temperature anomalies compared to the role of SSTs.

In contrast, the 2006 heat wave over the central and western United States (Fig. 5) is not captured by AM2.5 baseline simulations (pattern correlation is −0.31). We hence claim that SSTs are not critical for the summer of 2006. However, FLOR p2 is able to forecast most of the warm anomalies (pattern correlation is 0.25), although it overestimates the temperatures over the eastern United States. This overestimation could be the result of overestimation of temperature variability over eastern United States in p2 forecasts (not shown). Overall, both pattern and magnitudes of anomalies in p2 are more realistic than those in p1, which forecasts very weak warm anomalies over the western United States (pattern

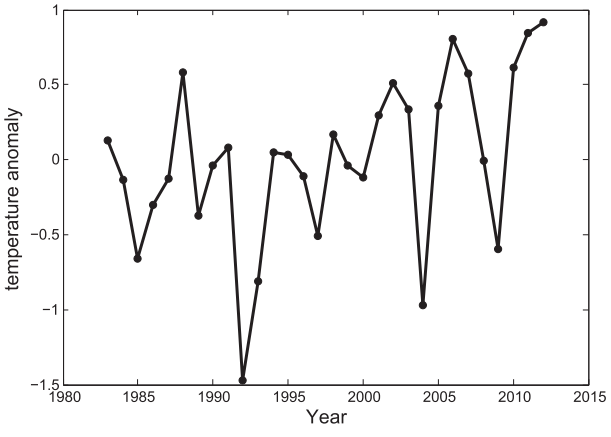

FIG. 3. The observed areal-averaged JJA 2-m temperature anomalies (in K) over the continental United States during 1983–2012 from the GHCN gridded v2 2-m temperature dataset.

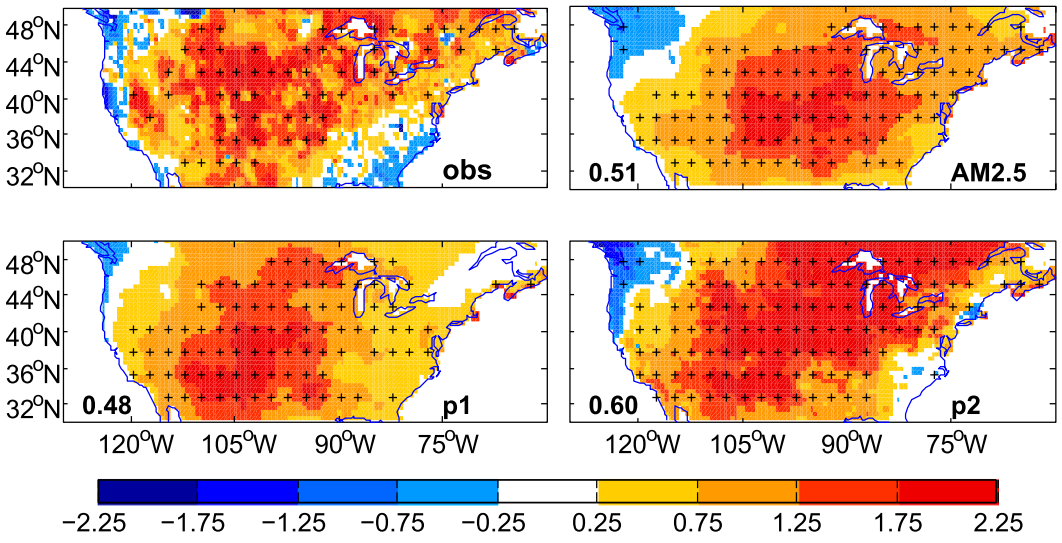

FIG. 4. The 2012 JJA 2-m temperature anomalies (in K, relative to 1983–2012) from the observations, ensemble mean of AM2.5 baseline simulations, and 12-member mean FLOR phase-1 and -2 forecasts initialized on 1 Jun 2012. The stippling indicates the amplitude of the anomalies exceeds one standard deviation in the observations, and is significant at the 5% significance level in AM2.5 baseline simulations and FLOR phase-1 and -2 forecasts. The numbers in the panels of AM2.5, FLOR p1, and FLOR p2 denote the pattern correlations with the observations.

correlation is 0.18). The improved forecasts in p2 over p1 indicate that atmospheric and land initial conditions are important for the summer of 2006.

a. The role of SSTs in the 2012 U.S. summer heat wave

To further diagnose the contributions of SSTs to the hot summer of 2012, we performed sensitivity experiments with AM2.5 by perturbing the SST forcing data. An additional experiment testing the role of direct radiative forcing in the 2012 U.S. summer heat wave was also conducted. For detailed experimental design, one can refer to section 2. Figure 6a displays the SST anomalies (relative to 1983–2012) in JJA 2012 from the observed SST data that are used to force AM2.5. Note that the spatial pattern of the SST anomalies after removing global mean SST anomalies is identical to the pattern shown in Fig. 6. The SST anomalies in 2012 show narrow warm anomalies over the eastern equatorial Pacific, a negative Pacific decadal oscillation (PDO) pattern over the North Pacific, and large warm

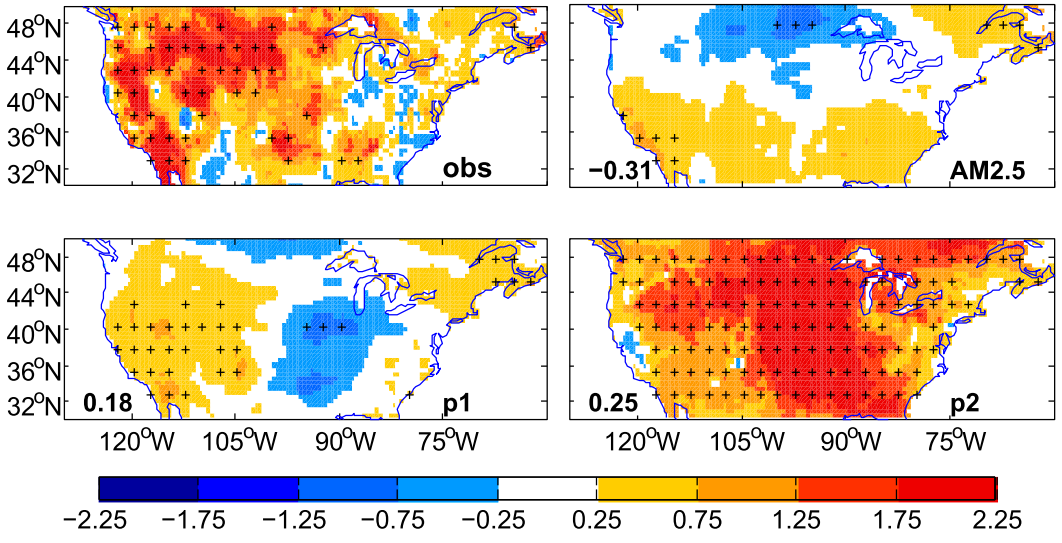

FIG. 5. As in Fig. 4, but for 2006.

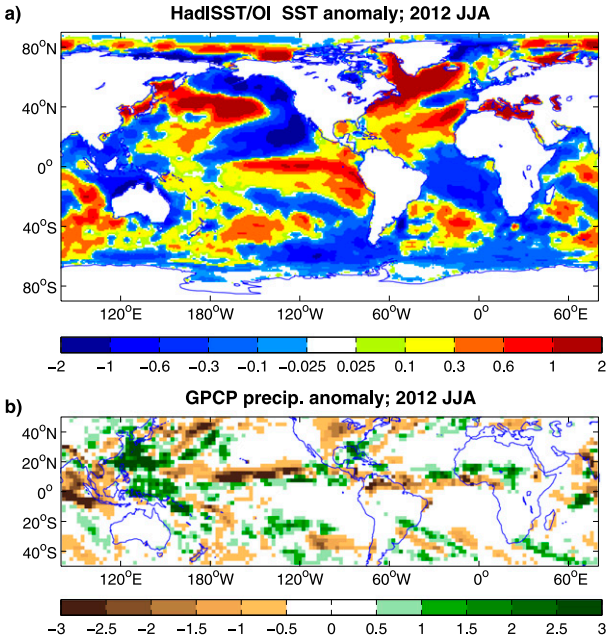

FIG. 6. (a) The 2012 JJA SST anomalies (in K) from the observed (HadISST1/OI) SST dataset used to force the AM2.5. (b) The 2012 JJA precipitation anomalies (in mm day^{-1}) from GPCP data. The anomalies of SST and precipitation are computed relative to the climatology of 1983–2012.

anomalies over the northwestern Atlantic. It is noteworthy that the SST structure over the tropical Pacific is not a conventional El Niño–like pattern, although there exist narrow warm anomalies over the eastern equatorial Pacific. The central Pacific over the tropics shows anomalous warm SSTs, contrary to the weak cold SST anomalies over the central and western equatorial Pacific during classic El Niño events (Curtis and Adler 2003; Wittenberg et al. 2006). The observed pattern of precipitation anomalies does not resemble the classic El Niño–related precipitation pattern either (Fig. 6b). Particularly, contrary to the dry conditions over the western equatorial Pacific during conventional El Niño events (Ropelewski and Halpert 1989, 1987; Wittenberg et al. 2006; Curtis and Adler 2003), it shows wet anomalies in JJA of 2012. The pattern of precipitation anomalies over the central and western tropical Pacific looks more like a La Niña pattern.

Figure 7 shows the 2012 JJA mean 2-m temperature anomalies over the continental United States from the observations, ensemble mean of AM2.5 baseline simulations, and sensitivity experiments that are due to the role of uniform global SST warming, direct radiative forcing, and SSTs in individual oceanic basins. The stippling areas indicate that temperature anomalies are significant at 5% level for model experiments, and exceed one standard deviation in the observations. The uniform global SST warming plays a role in the northeastern United States. The influence of direct radiative forcing is weak and insignificant at the 5% level. The impacts of SSTs in the tropical Atlantic, tropical Pacific, North Pacific, and North Atlantic are on the east, midsoutheast, north, and west of the United States, respectively. Our results from the North Atlantic experiment agree with the findings by Wang et al. (2014), with the NASA Goddard Earth Observing System, version 5 (GEOS-5), atmospheric general circulation model. The roles played by SSTs in other basins do not appear to be consistent with those in Wang et al. (2014), which is presumably due to the differences in many aspects between these two studies: 1) the area of domains (the size of each ocean domain was defined differently); 2) months (Wang et al. 2014 showed June–July anomalies, rather than JJA anomalies in this study); 3) no removal of uniform global SST warming in Wang et al. (2014); and 4) GEOS-5 did not simulate the warmth over the eastern United States in 2012, it only simulated the warm anomalies over the western United States.

The pattern correlations between the observed temperature anomalies over the United States and the temperature anomalies from AM2.5 baseline simulations, as well as from sensitivity experiments for each ensemble member (open circle) and ensemble mean (solid dot) are shown in Fig. 8a. According to the correlation coefficients of ensemble mean, it is not surprising that the AM2.5 baseline simulations, which consist of historical SST forcing from all ocean basins, global SST warming effects, and influence of direct radiative forcing display the largest pattern correlation (0.51) with the observations. In addition, the areal-averaged temperature anomaly over the United States from the ensemble mean of AM2.5 baseline simulations (red solid dot) is very close to the observed temperature anomaly (black dot), although the anomalies from individual ensemble members show a large spread (Fig. 8b). In sensitivity experiments, high pattern correlations are found for the patterns due to the North Pacific, tropical Pacific, and radiative forcing. The lowest pattern correlation is shown in the North Atlantic experiment. Although the pattern caused by direct radiative forcing shows relatively high pattern correlation, its magnitude is the smallest among all experiments, consistent with the weak temperature anomaly pattern shown in Fig. 7. The contributions from SST warming, and individual oceanic basins to ensemble mean temperature anomalies are comparable, with slightly more contributions from the topical Pacific, tropical Atlantic, and North Pacific. Large ensemble spreads are spotted for both the amplitudes of temperature anomalies and pattern correlations in all sensitivity experiments, indicated by open circles. For instance, in the tropical Atlantic experiment, three ensemble members show

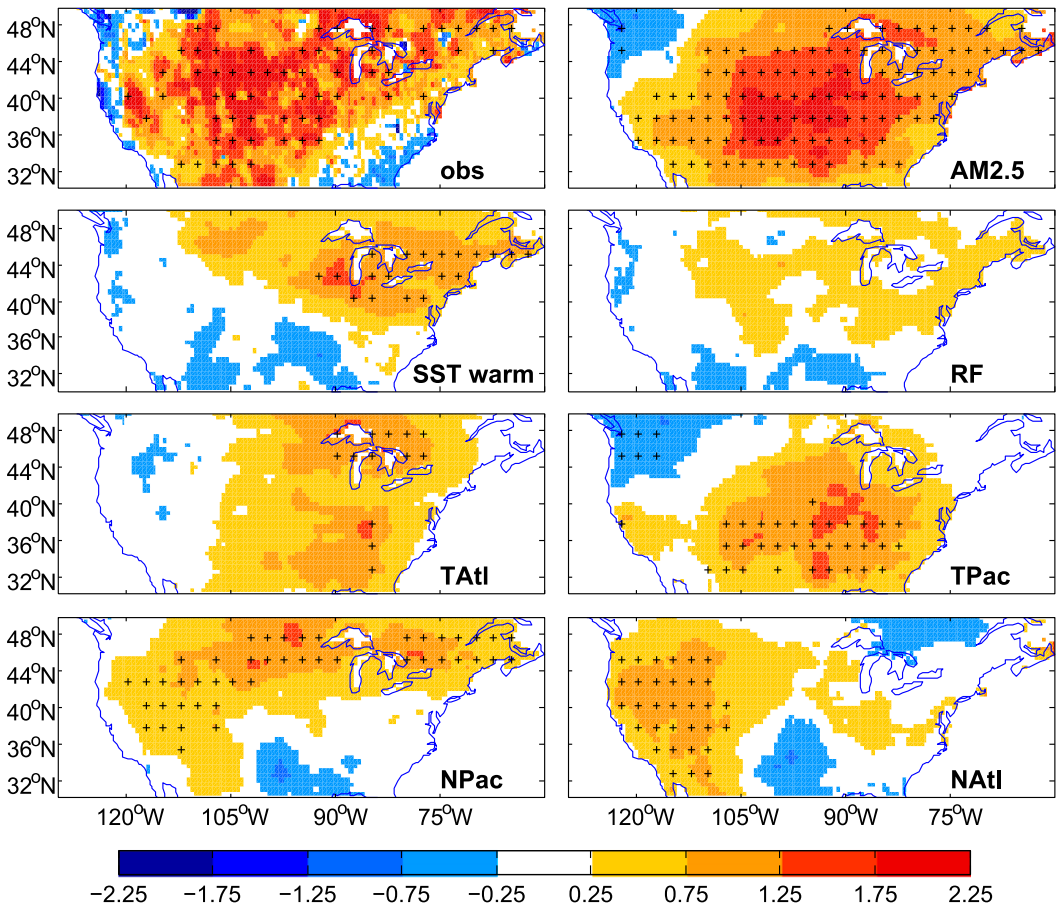

FIG. 7. The 2012 JJA mean 2-m temperature anomalies (in K, relative to 1983–2012) from the observations, ensemble mean of AM2.5 baseline simulations, and sensitivity experiments that are due to the role of uniform global SST warming, direct radiative forcing, and SSTs in the tropical Atlantic, tropical Pacific, North Pacific, and North Atlantic. The stippling indicates that the temperature anomalies are significant at the 5% level for model simulations and exceed one standard deviation in the observations.

negative pattern correlations although the overall pattern correlation from ensemble mean (solid dot) is positive.

b. *The roles of atmospheric and land initial conditions in the 2006 U.S. summer heat wave*

Before assessing the roles of atmospheric and land conditions in the 2006 U.S. summer heat wave using FLOR p2, we first examine the 2006 1 June land initial conditions for the JJA prediction. The soil moisture content shows negative anomalies over the central and southeastern United States in FLOR p2, similar to those from GLDAS (Fig. 9). Such dry land conditions could contribute to the temperature predictions of the following summer.

Figure 10 shows the 2006 JJA 2-m temperature and 500-hPa height anomalies due to the atmospheric and land initial conditions, as well as those from the observations and original (also called ''baseline'') p2 forecasts. The role of atmosphere (land) is estimated as the difference between the baseline p2 forecasts and the forecasts from the sensitivity experiment with random atmospheric (land) initial information. The atmospheric initial conditions contribute to the warm anomalies over the central and northwestern United States. The associated 500-hPa height shows positive anomalies over North America, which significantly resemble the height anomalies from MERRA and the baseline p2 forecasts. The high pressure center over the United States produces subsidence, warm-air advection, light wind, and clear skies that favor the hot conditions (Black et al. 2004; Meehl and Tebaldi 2004). The land initial conditions lead to warm anomalies primarily over the central and eastern United States, with the largest anomalies over the southeast. This result might be related to the earlier dry land initial conditions over the southeastern United States as shown in Fig. 9. In other words, the dry land initial conditions could provide prior conditions for the development of warm anomalies over the United

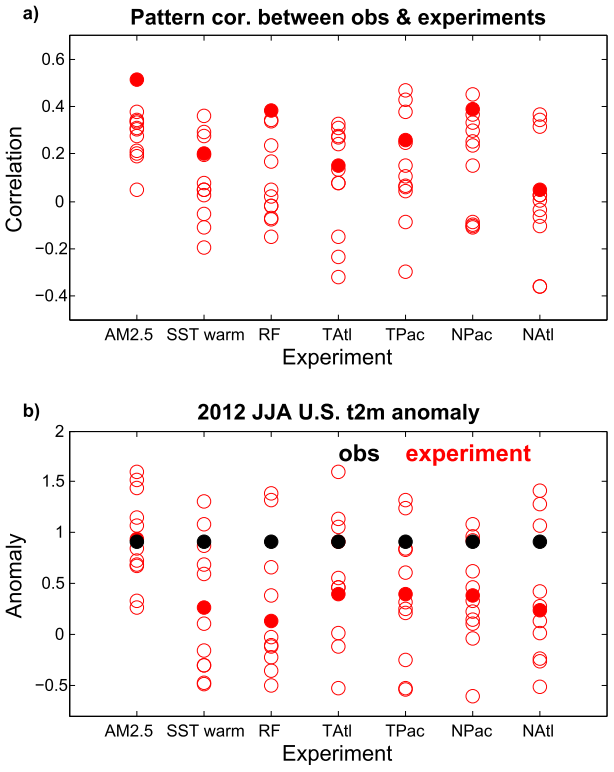

FIG. 8. (a) The pattern correlation of 2012 JJA U.S. 2-m temperature anomalies between the observations and AM2.5 baseline simulations, and sensitivity experiments due to the role of uniform global SST warming, direct radiative forcing, and SSTs in the tropical Atlantic, tropical Pacific, North Pacific, and North Atlantic. (b) The areal-averaged 2012 JJA U.S. 2-m temperature anomalies (in K) in the observations, AM2.5 baseline simulations, and sensitivity experiments. The red solid dot denotes the result from ensemble mean and the red open circles denote the results from ensemble members. The black solid dot indicates the observed temperature anomaly. The anomalies are computed relative to the climatology of 1983–2012.

States. The spatial structure of temperature anomalies due to land initial conditions does not agree with the observed structure that has largest warm anomalies over central and western United States, and the corresponding 500-hPa height pattern due to land initial conditions displays weaker anomalies compared to that due to atmospheric initial conditions. We thus claim that land initial conditions play a minor role, while the atmospheric initial conditions play a major role in the hot summer of 2006.

Our conclusion that atmospheric initial conditions are critical for heat wave predictions on seasonal time scales may seem contrary to the commonsense that atmospheric predictability is limited to a few weeks. However, the predictability from atmospheric initial conditions can be reflected in monthly or seasonal means, because of the predictability of low-frequency planetary waves (Shukla 1981). As shown in Fig. 11, the

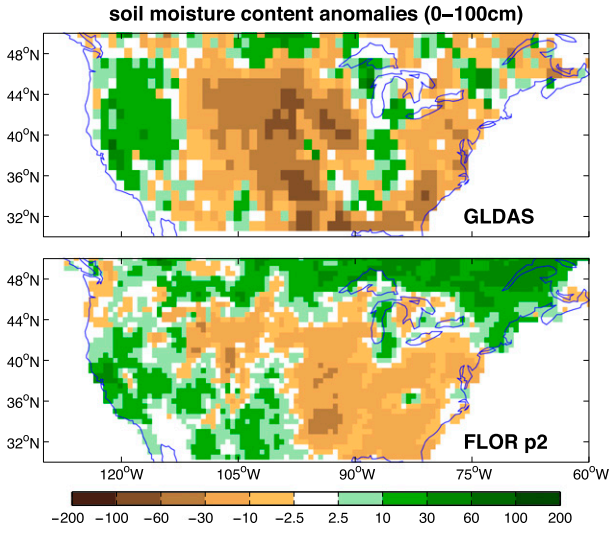

FIG. 9. The 1 Jun 2006 initial conditions of soil moisture content (in $kg\,m^{-2}$) anomalies over the United States for FLOR phase-2 forecasts, and the 1 Jun 2006 soil moisture content anomalies from GLDAS Noah land surface model V3.3.

atmospheric initial conditions play a significant role in June 2006, as indicated by the large similarities of 500-hPa height between the observations and FLOR p2 forecasts. However, the contribution from atmospheric initial conditions is much less in July 2006 when forecasting from June 2006. These results suggest that the contribution of atmospheric initial conditions to seasonal predictions is mostly in the first month.

c. *The role of radiative forcing changes in multidecadal variations of U.S. summer heat waves*

Having discussed the contributions of SSTs, atmospheric, and land initial conditions to U.S. summer heat waves, a question of greatest concern is whether a summer heat wave as severe as the one observed in 2012 can be anticipated. In this section, we attempt to investigate the role of changes of radiative forcing in the multidecadal variations of U.S. summer heat waves. Specifically, we diagnose the probability of areal-averaged U.S. summer temperature anomalies exceeding the observed 2012 temperature anomaly on multidecadal time scales utilizing the FLOR 30-member simulations from 1941 to 2050. As these simulations are forced with historical forcing (before 2005) and RCP4.5 forcing (after 2005), the multidecadal variations of heat waves in these ensemble simulations are attributable to the changes in radiative forcing.

Figure 12 displays the probability of simulated areal-averaged U.S. 2-m temperature anomalies exceeding the observed 2012 U.S. JJA temperature anomaly in any 30-yr chunks. To minimize the sampling error, starting

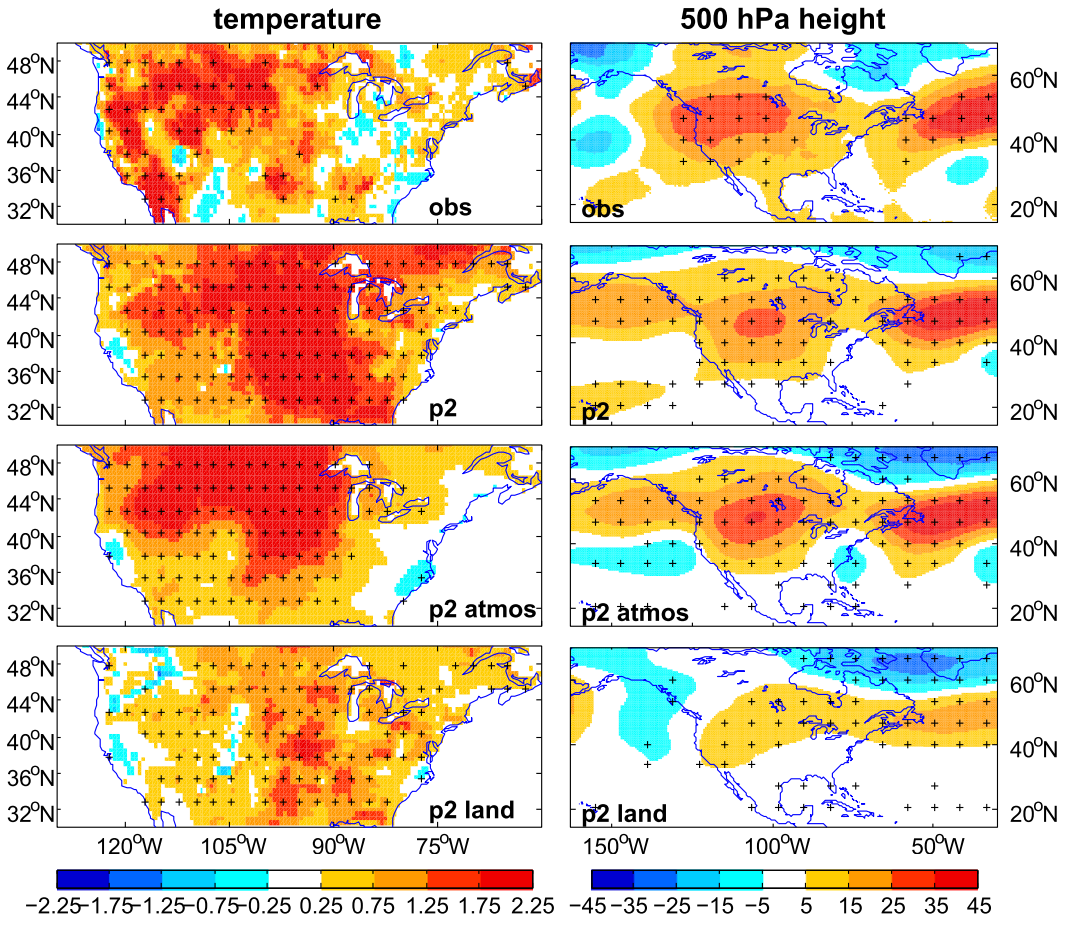

FIG. 10. The 2006 JJA (left) 2-m temperature anomalies (in K) and (right) 500-hPa height anomalies (in m) in the observations, ensemble mean of the original (i.e., baseline) FLOR phase-2 forecasts, and those due to atmospheric and land initial conditions. The anomalies due to atmospheric and land initial conditions for both fields are derived relative to the climatology of 1983–2012 from the baseline FLOR phase-2 forecasts. The forecasts from the baseline FLOR phase-2 and sensitivity experiments are initialized on 1 Jun 2006. The stippling indicates that the anomalies are significant at the 5% level in FLOR phase-2 forecasts and exceed one standard deviation in the observations.

from 1941, the last 20 years of each 30-yr chunk overlap with the first 20 years of the following 30-yr chunk (i.e., 1941–70, 1951–80, . . . , 2021–50). The years shown in the x axis of the figure represent the centers of each 30-yr chunk (e.g., 1955 indicates the 30-yr chunk of 1941–70). For each 30-yr chunk, 900 (30 members $\times$ 30 yr) samples are available to compute the probability. To avoid the influence of bias in the model simulations, we calculated the rank of the observed 2012 JJA temperature anomalies during 1983–2012 in the observations, and then calibrated the threshold of temperature anomalies in the ensemble simulations as the simulated temperature anomalies of the same rank as in the observations during 1983–2012. The probability of U.S. JJA temperature anomalies exceeding the calibrated observed 2012 JJA temperature anomalies increases significantly with time after the period of 1981–2010 (centered at 1995) as a result of radiative forcing changes (black line). It is less than 5% during 1981–2010, but will reach ~40% during the decades of 2021–50. These results agree with the findings by Meehl and Tebaldi (2004) that heat waves will be more frequent in the twenty-first century.

Another interesting question is whether the probability of the occurrence rate of heat waves can be modulated by natural variability. We show in Fig. 12 the conditional probability of temperature anomalies in multidecadal simulations higher than the observed 2012 temperature anomalies in El Niño (red line) and La Niña (blue line) years, respectively. Here, the El Niño and La Niña years in the model simulations are defined as the years with normalized and detrended Niño index exceeding one standard deviation, and they are defined based on SSTs over Niño-3 (eastern Pacific) and Niño-4 (central Pacific) regions separately. In both cases, the probability of U.S. summer heat waves increases during La Niña years, but decreases during El Niño years. These results are

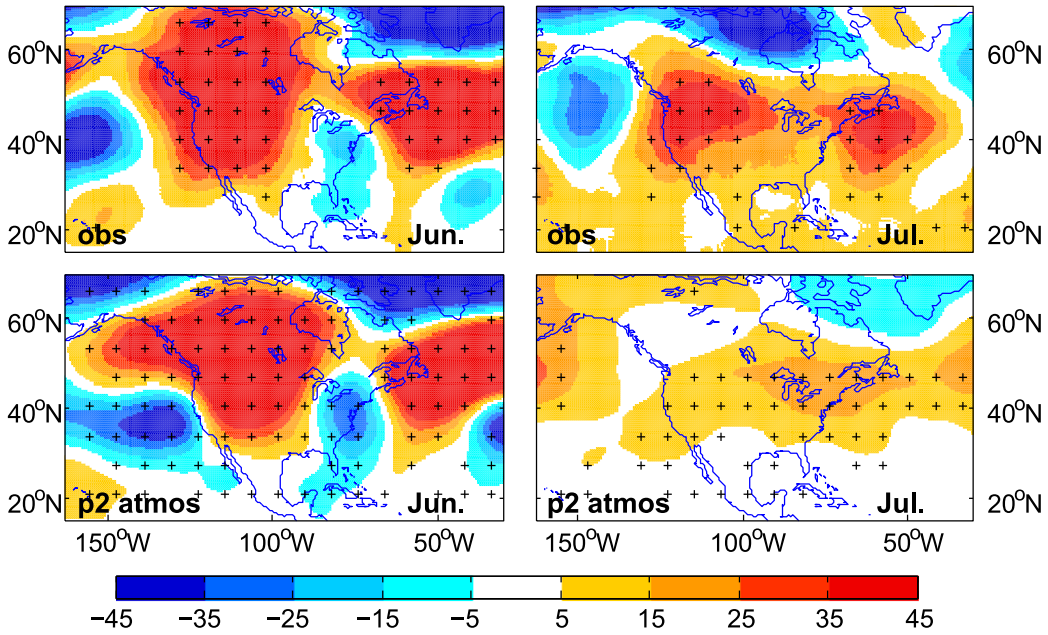

FIG. 11. The 500-hPa height anomalies (in m) for (left) June and (right) July 2006 in the observations and those due to atmospheric initial conditions in FLOR phase-2 forecasts that initialized on 1 Jun 2006. The anomalies due to atmospheric initial conditions are derived relative to the climatology of 1983–2012 from the baseline FLOR phase-2 forecasts. The stippling indicates that the anomalies are significant at the 5% level in FLOR phase-2 forecasts and exceed one standard deviation in the observations.

consistent with the findings in previous studies (Wang et al. 2007; Koster et al. 2009; Hoerling et al. 2013). As the probability increases with time, the range of the probability between El Niño and La Niña years, indicated by the percentage difference between La Niña and El Niño years, also increases (bottom panels). An important feature of the El Niño/La Niña impact is that the impact from the Niño-4 (5°S–5°N, 160°E–150°W) region is generally greater than the impact from the Niño-3 (5°S–5°N, 90°–150°W) region, particularly over the decades of 2011–50 (i.e., the central and western equatorial Pacific plays a more important role than the eastern equatorial Pacific in U.S. summer heat waves). These conclusions support the results discussed above that the 2012 JJA SST and precipitation anomalies over the central and western United States are more like the La Niña–related pattern, and La Niña events favor the occurrence of heat waves. As found by Yeh et al. (2009) the frequency of central Pacific El Niño increases in a warming climate, so the scenario of the impacts of Niño-4 on U.S. heat waves would occur more frequently in future. The impacts of other natural variability, such as PDO and Atlantic multidecadal oscillation (AMO) on U.S. summer heat waves are also explored (not shown), but no robust conclusions can be drawn.

The spatial structure of temperatures influenced by El Niño/La Niña events is shown in Fig. 13, which displays the composite of temperature anomalies during La Niña–El Niño years. Here, the El Niño/La Niña events are defined according to the SSTs in Niño-4 region. A very similar spatial structure of temperature anomalies is found when defining El Niño/La Niña events based on SSTs in the Niño-3 region, but for weaker magnitudes (not shown). This further supports our conclusion that the central and western tropical Pacific plays a more important role than the eastern tropical Pacific in U.S. summer heat waves. Warm temperature anomalies occur over most of the United States during La Niña years, but only for the northwestern United States. The largest warm anomalies are located in the central United States, where the La Niña/El Niño events have the most significant impacts.

4. Summary and discussion

To understand the causes of U.S. summer warming episodes (i.e., heat waves), we investigated systematically the roles played by radiative forcing, SST boundary conditions, and atmospheric/land initial conditions in U.S. summer heat waves. Two contrasting case studies reveal that SSTs play a critical role in the hot summer of 2012, while atmospheric and land initial conditions are critical for the 2006 U.S. summer heat wave. A series of sensitivity experiments were conducted to explore the roles of SSTs in individual ocean basins, uniform global SST warming, and direct radiative forcing in the 2012

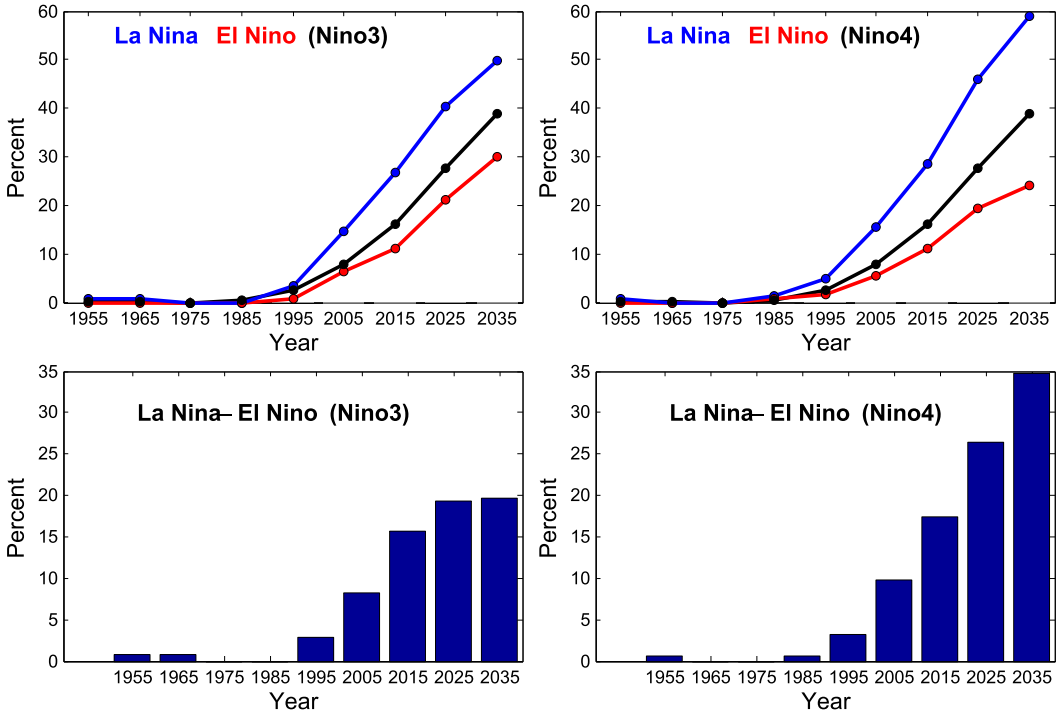

FIG. 12. (top) The percentage of areal-averaged U.S. JJA 2-m temperature anomalies in the 30-member multidecadal simulations exceeding the observed 2012 JJA temperature anomaly averaged over the United States for each 30-yr chunk (black), and the percentage during El Niño (red) and La Niña (blue) years for (left) Niño-3 and (right) Niño-4 regions. (bottom) The difference of percentage between La Niña and El Niño years.

U.S. summer heat wave, and to estimate the contributions from atmospheric and land initial conditions in the 2006 U.S. summer heat wave. Our results show that the SSTs over the North Atlantic, tropical Atlantic, tropical Pacific, North Pacific, and uniform global SST warming contribute to the 2012 JJA warm temperature anomalies in the west, east, midsoutheast, north, and northeast of the United States, respectively. Compared to the contributions from SSTs to the heat wave in 2012, the contributions from direct radiative forcing are not significant. For the hot summer of 2006, the atmospheric (land) initial conditions contribute to the strong (weak) positive temperature anomalies over the central and northwest (east) region of the United States. The high temperature anomalies are often associated with high pressure center over the United States, which provides subsidence, warm-air advection, light wind, and clear skies that favor the hot conditions.

Because of the changes in radiative forcing, the probability of areal-averaged United States, JJA temperature anomalies exceeding the observed 2012 JJA temperature anomaly increases with time, particularly in the early twenty-first century. The probability increases from ~5% in the beginning of the twenty-first century to ~40% by the middle of the twenty-first century. The occurrence rate of U.S. summer heat waves can be modulated by natural variability—El Niño and La Niña. During La Niña years, the probability increases, but decreases in El Niño years. We found that the central United States is the place where the temperatures are significantly impacted by El Niño/La Niña. The impact from the central/western tropical Pacific (Niño-4 region) appears to be higher than the impact from the eastern tropical Pacific (Niño-3 region).

Our results suggest that atmospheric and land initial conditions, SSTs, and radiative forcing are all important

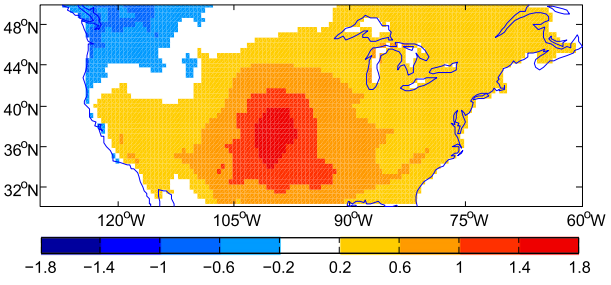

FIG. 13. The composite of 2-m temperature anomalies (in K) for La Niña–El Niño events from the 30-member multidecadal simulations. The La Niña and El Niño events are defined based on the SSTs over Niño-4 region.

drivers of, and sources of predictability for U.S. summer heat waves. Therefore, the development of coupled ocean and atmosphere data assimilation system, rather than initializing the ocean alone, would be helpful for U.S. heat wave predictions. This research provides a scientific basis for seasonal predictions of U.S. summer heat waves and adaptation to climate change, in spite of the limitations of the study. The results might be model dependent. Further study diagnosing the model biases would be beneficial.

Acknowledgments. The authors thank Drs. Nathaniel Johnson and Jonghun Kam for insightful comments in an earlier version of this manuscript. We also thank three anonymous reviewers for their constructive comments. This work is supported in part by National Oceanic and Atmospheric Administration (NOAA) Climate Program Office. Drs. G. Vecchi and X. Yang are supported by NOAA/OAR under the auspices of the National Earth System Prediction Capability (National ESPC).

REFERENCES

Adler, R., and Coauthors, 2003: The Version-2 Global Precipitation Climatology Project (GPCP) monthly precipitation analysis (1979–present). *J. Hydrometeor.*, **4**, 1147–1167, doi:10.1175/1525-7541(2003)004<1147:TVGPCP>2.0.CO;2.

Black, E., M. Blackburn, G. Harrison, and J. Methven, 2004: Factors contributing to the summer 2003 European heat wave. *Weather*, **59**, 217–223, doi:10.1256/wea.74.04.

Chang, Y.-S., S. Zhang, A. Rosati, T. L. Delworth, and W. F. Stern, 2013: An assessment of oceanic variability for 1960–2010 from the GFDL ensemble coupled data assimilation. *Climate Dyn.*, **40**, 775–803, doi:10.1007/s00382-012-1412-2.

Changnon, S., K. Kunkel, and B. Reinke, 1996: Impacts and responses to the 1995 heat wave: A call to action. *Bull. Amer. Meteor. Soc.*, **77**, 1497–1506, doi:10.1175/1520-0477(1996)077<1497:IARTTH>2.0.CO;2.

Chen, M., P. Xie, J. E. Janowiak, and P. A. Arkin, 2002: Global land precipitation: A 50-yr monthly analysis based on gauge observations. *J. Hydrometeor.*, **3**, 249–266, doi:10.1175/1525-7541(2002)003<0249:GLPAYM>2.0.CO;2.

Curtis, S., and R. F. Adler, 2003: Evolution of El Niño–precipitation relationships from satellites and gauges. *J. Geophys. Res.*, **108**, 4153, doi:10.1029/2002JD002690.

Delworth, T. L., and Coauthors, 2006: GFDL's CM2 global coupled climate models. Part I: Formulation and simulation characteristics. *J. Climate*, **19**, 643–674, doi:10.1175/JCLI3629.1.

——, and Coauthors, 2012: Simulated climate and climate change in the GFDL CM2.5 high-resolution coupled climate model. *J. Climate*, **25**, 2755–2781, doi:10.1175/JCLI-D-11-00316.1.

Dole, R., and Coauthors, 2011: Was there a basis for anticipating the 2010 Russian heat wave? *Geophys. Res. Lett.*, **38**, L06702, doi:10.1029/2010GL046582.

——, and Coauthors, 2014: The making of an extreme event: Putting the pieces together. *Bull. Amer. Meteor. Soc.*, **95**, 427–440, doi:10.1175/BAMS-D-12-00069.1.

Fan, Y., and H. Van den Dool, 2008: A global monthly land surface air temperature analysis for 1948–present. *J. Geophys. Res.*, **113**, D01103, doi:10.1029/2007JD008470.

Fischer, E. M., S. I. Seneviratne, P. L. Vidale, D. Lüthi, and C. Schär, 2007: Soil moisture–atmosphere interactions during the 2003 European summer heat wave. *J. Climate*, **20**, 5081–5099, doi:10.1175/JCLI4288.1.

Frich, P., L. V. Alexander, P. Della-Marta, B. Gleason, M. Haylock, A. M. G. K. Tank, and T. Peterson, 2002: Observed coherent changes in climatic extremes during the second half of the twentieth century. *Climate Res.*, **19**, 193–212, doi:10.3354/cr019193.

Gnanadesikan, A., and Coauthors, 2006: GFDL's CM2 global coupled climate models. Part II: The baseline ocean simulation. *J. Climate*, **19**, 675–697, doi:10.1175/JCLI3630.1.

Hansen, J., M. Sato, and R. Ruedy, 2012: Perception of climate change. *Proc. Natl. Acad. Sci. USA*, **109**, E2415–E2423, doi:10.1073/pnas.1205276109.

Hoerling, M., and Coauthors, 2013: Anatomy of an extreme event. *J. Climate*, **26**, 2811–2832, doi:10.1175/JCLI-D-12-00270.1.

Huang, J., and H. Van den Dool, 1993: Monthly precipitation–temperature relations and temperature prediction over the United States. *J. Climate*, **6**, 1111–1132, doi:10.1175/1520-0442(1993)006<1111:MPTRAT>2.0.CO;2.

Hurrell, J. W., J. J. Hack, D. Shea, J. M. Caron, and J. Rosinsk, 2008: A new sea surface temperature and sea ice boundary dataset for the Community Atmosphere Model. *J. Climate*, **21**, 5145–5153, doi:10.1175/2008JCLI2292.1.

Jia, L., and Coauthors, 2015: Improved seasonal prediction of temperature and precipitation over land in a high-resolution GFDL climate model. *J. Climate*, **28**, 2044–2062, doi:10.1175/JCLI-D-14-00112.1.

Kirtman, B. P., and Coauthors, 2014: The North American Multimodel Ensemble: Phase-1 seasonal-to-interannual prediction; Phase-2 toward developing intraseasonal prediction. *Bull. Amer. Meteor. Soc.*, **95**, 585–601, doi:10.1175/BAMS-D-12-00050.1.

Koster, R. D., H. Wang, S. D. Schubert, M. J. Suarez, and S. Mahanama, 2009: Drought-induced warming in the continental United States under different SST regimes. *J. Climate*, **22**, 5385–5400, doi:10.1175/2009JCLI3075.1.

Meehl, G. A., and C. Tebaldi, 2004: More intense, more frequent, and longer lasting heat waves in the 21st century. *Science*, **305**, 994–997, doi:10.1126/science.1098704.

Meinshausen, M., and Coauthors, 2011: The RCP greenhouse gas concentrations and their extensions from 1765 to 2300. *Climate Change*, **109**, 213–241, doi:10.1007/s10584-011-0156-z.

Murakami, H., G. A. Vecchi, T. Delworth, K. Paffendorf, R. Gudgel, L. Jia, and F. Zeng, 2015: Investigating the influence of anthropogenic forcing and natural variability on the 2014 Hawaiian hurricane season. *Bull. Amer. Meteor. Soc.*, **96**, S115–S119, doi:10.1175/BAMS-D-15-00119.1.

Perkins, S. E., and L. V. Alexander, 2013: On the measurement of heat waves. *J. Climate*, **26**, 4500–4517, doi:10.1175/JCLI-D-12-00383.1.

Rayner, N. A., D. E. Parker, E. B. Horton, C. K. Folland, L. V. Alexander, D. P. Rowell, E. C. Kent, and A. Kaplan, 2003: Global analyses of sea surface temperature, sea ice, and night marine air temperature since the late nineteenth century. *J. Geophys. Res.*, **108**, 4407, doi:10.1029/2002JD002670.

Rienecker, M. M., and Coauthors, 2011: MERRA: NASA's Modern-Era Retrospective Analysis for Research and Applications. *J. Climate*, **24**, 3624–3648, doi:10.1175/JCLI-D-11-00015.1.

Robine, J.-M., S. L. K. Cheung, S. L. Roy, H. V. Oyen, C. Griffiths, J.-P. Michel, and F. R. Herrmann, 2008: Death toll exceeded

70,000 in Europe during the summer of 2003. *C. R. Biol.*, **331**, 171–178, doi:10.1016/j.crvi.2007.12.001.

Robinson, P. J., 2001: On the definition of a heat wave. *J. Appl. Meteor.*, **40**, 762–775, doi:10.1175/1520-0450(2001)040<0762:OTDOAH>2.0.CO;2.

Rodell, M., and Coauthors, 2004: The global land data assimilation system. *Bull. Amer. Meteor. Soc.*, **85**, 381–394, doi:10.1175/BAMS-85-3-381.

Ropelewski, C., and M. Halpert, 1987: Global and regional scale precipitation patterns associated with the El Niño/Southern Oscillation. *Mon. Wea. Rev.*, **115**, 1606–1626, doi:10.1175/1520-0493(1987)115<1606:GARSPP>2.0.CO;2.

——, and ——, 1989: Precipitation patterns associated with the high index phase of the Southern Oscillation. *J. Climate*, **2**, 268–284, doi:10.1175/1520-0442(1989)002<0268:PPAWTH>2.0.CO;2.

Schär, C., P. L. Vidale, D. Lüthi, C. Frei, C. Häberli, M. A. Liniger, and C. Appenzeller, 2004: The role of increasing temperature variability in European summer heatwaves. *Nature*, **427**, 332–336, doi:10.1038/nature02300.

Schubert, S. D., H. Wang, R. D. Koster, M. J. Suarez, and P. Ya. Groisman, 2014: Northern Eurasian heat waves and droughts. *J. Climate*, **27**, 3169–3207, doi:10.1175/JCLI-D-13-00360.1.

Shukla, J., 1981: Dynamical predictability of monthly means. *Mon. Wea. Rev.*, **38**, 2547–2572, doi:10.1175/1520-0469(1981)038<2547:DPOMM>2.0.CO;2.

Stott, P. A., D. A. Stone, and M. R. Allen, 2004: Human contribution to the European heatwave of 2003. *Nature*, **432**, 610–614, doi:10.1038/nature03089.

Vecchi, G., and Coauthors, 2014: On the seasonal forecasting of regional tropical cyclone activity. *J. Climate*, **27**, 7994–8016, doi:10.1175/JCLI-D-14-00158.1.

Wang, H., S. Schubert, R. Koster, Y.-G. Ham, and M. Suarez, 2014: On the role of SST forcing in the 2011 and 2012 extreme U.S. heat and drought: A study in contrasts. *J. Hydrometeor.*, **15**, 1255–1273, doi:10.1175/JHM-D-13-069.1.

Wang, Z., C.-P. Chang, and B. Wang, 2007: Impacts of El Niño and La Niña on the U.S. climate during northern summer. *J. Climate*, **20**, 2165–2177, doi:10.1175/JCLI4118.1.

Wittenberg, A. T., A. Rosati, N.-C. Lau, and J. J. Ploshay, 2006: GFDL's CM2 global coupled climate models. Part III: Tropical Pacific climate and ENSO. *J. Climate*, **19**, 698–722, doi:10.1175/JCLI3631.1.

Yang, X., and Coauthors, 2015: Seasonal predictability of extratropical storm tracks in GFDL's high-resolution climate prediction model. *J. Climate*, **28**, 3592–3611, doi:10.1175/JCLI-D-14-00517.1.

Yeh, S.-W., J.-S. Kug, B. Dewitte, M.-H. Kwon, B. P. Kirtman, and F.-F. Jin, 2009: El Niño in a changing climate. *Nature*, **461**, 511–514, doi:10.1038/nature08316.

Zhang, S., and A. Rosati, 2010: An inflated ensemble filter for ocean data assimilation with a biased coupled GCM. *Mon. Wea. Rev.*, **138**, 3905–3931, doi:10.1175/2010MWR3326.1.

——, M. J. Harrison, A. Rosati, and A. T. Wittenberg, 2007: System design and evaluation of coupled ensemble data assimilation for global oceanic climate studies. *Mon. Wea. Rev.*, **135**, 3541–3564, doi:10.1175/MWR3466.1.